Elastic properties of suspended multilayer WSe2

AIP | Applied Physics Letters

Elastic properties of suspended multilayer WSe2

Rui Zhang, Vasileios Koutsos, and Rebecca Cheung

Citation: Applied Physics Letters **108**, 042104 (2016); doi: 10.1063/1.4940982
View online: http://dx.doi.org/10.1063/1.4940982
View Table of Contents: http://scitation.aip.org/content/aip/journal/apl/108/4?ver=pdfcov
Published by the AIP Publishing

Elastic properties of suspended multilayer WSe_2

Rui Zhang,[1,a] Vasileios Koutsos,[2] and Rebecca Cheung[1]
[1]*Scottish Microelectronics Centre, Alexander Crum Brown Road, The University of Edinburgh, King's Buildings, Edinburgh EH9 3FF, United Kingdom*
[2]*Institute for Materials and Processes, School of Engineering, The University of Edinburgh, King's Buildings, Edinburgh EH9 3FB, United Kingdom*

(Received 12 November 2015; accepted 17 January 2016; published online 27 January 2016)

We report the experimental determination of the elastic properties of suspended multilayer WSe_2, a promising two-dimensional (2D) semiconducting material combined with high optical quality. The suspended WSe_2 membranes have been fabricated by mechanical exfoliation of bulk WSe_2 and transfer of the exfoliated multilayer WSe_2 flakes onto SiO_2/Si substrates pre-patterned with hole arrays. Then, indentation experiments have been performed on these membranes with an atomic force microscope. The results show that the 2D elastic modulus of the multilayer WSe_2 membranes increases linearly while the prestress decreases linearly as the number of layers increases. The interlayer interaction in WSe_2 has been observed to be strong enough to prevent the interlayer sliding during the indentation experiments. The Young's modulus of multilayer WSe_2 (167.3 ± 6.7 GPa) is statistically independent of the thickness of the membranes, whose value is about two thirds of other most investigated 2D semiconducting transition metal dichalcogenides, namely, MoS_2 and WS_2. Moreover, the multilayer WSe_2 can endure ~12.4 GPa stress and ~7.3% strain without fracture or mechanical degradation. The 2D WSe_2 can be an attractive semiconducting material for application in flexible optoelectronic devices and nano-electromechanical systems.
 [http://dx.doi.org/10.1063/1.4940982]

Two-dimensional (2D) materials have triggered great interest in the application of flexible electronic devices and nano-electromechanical systems (NEMS) in recent years, due to their unique physical properties (ultralow weight, high Young's modulus, and high strength) and flexibility. The most widely studied 2D material so far is graphene because of its extraordinary physical properties (Young's modulus of ~1 TPa and breaking strength of 100–120 GPa)[1,2] and high mobility,[3] and there has been a great quantity of research related to graphene based flexible devices[4,5] and NEMS.[6–8] However, pristine graphene does not have a bandgap,[9] which limits its applications in certain fields requiring a semiconducting material. As a potential substitute material of graphene, the 2D semiconducting transition metal dichalcogenides (TMDs) with an intrinsic bandgap,[10,11] such as MoS_2, WS_2, and WSe_2, attract increasing attention, especially in electronic and optoelectronic applications.[12–15]

2D WSe_2 (normally exfoliated from the synthetic WSe_2 crystals grown by chemical vapor transport method), as a semiconductor with high optical quality (much higher electroluminescence efficiency than natural MoS_2;[16,17] higher photoluminescence (PL) intensity than synthetic WS_2 and natural MoS_2;[10] higher photo-conversion efficiency than natural MoS_2[18,19]), is a promising 2D material for application in optoelectronic devices, such as photodetectors, photovoltaics, and light-emitting diodes (LEDs). Simultaneously, under tensile strain, monolayer WSe_2 remains a direct bandgap material with a bandgap decrease rate of ~8 meV/% and multilayer WSe_2 undergoes an indirect to direct bandgap transition,[20] while monolayer MoS_2 shows a direct to indirect bandgap transition with a higher bandgap decrease rate of ~45 meV/% (PL intensity decreases rapidly with strain).[21] Since the strain induced bandgap change will influence the resistivity of 2D materials,[22] the smaller rate of bandgap change under strain of 2D WSe_2 makes it a great contender for flexible electronic/optoelectronic device applications. Although a lot of research has been done to study the electrical and optical properties of the 2D TMDs,[23–28] the investigations relevant to quantifying their mechanical properties experimentally (MoS_2[29–31] and WS_2[31]) are still quite few. So far, the experimental measurement of elastic properties of 2D WSe_2 has not been reported yet. In this work, we report the in-plane elastic properties of exfoliated multilayer WSe_2 extracted from nanoindentation experiments. Our experiment aims to pave the way for the design and fabrication of a 2D WSe_2 based flexible device and NEMS.

The indentation experiments have been performed on multilayer WSe_2 membranes suspended over circular holes with an atomic force microscope (AFM). First, 280 nm SiO_2 has been grown on Si substrates by thermal oxidation, which gives the optimal color contrast between WSe_2 flakes and the substrates.[32,33] Then, the SiO_2 layers have been patterned with circular hole (1.55 μm and 2.6 μm in diameter, 220 nm in depth) arrays by photolithography and reactive ion etching (see Fig. S1 of the supplementary material).[34] After etching, the photoresist has been stripped by sonication in acetone, isopropyl alcohol (IPA), and de-ionized (DI) water sequentially. Then, the substrates have been soaked in Piranha

[a]Author to whom correspondence should be addressed. Electronic mail: rui.zhang@ed.ac.uk

solution for 30 min and rinsed in DI water to remove organic residues, followed by O_2 plasma treatment to increase the interaction between WSe_2 flakes and SiO_2 surface by removing the ambient adsorbates on SiO_2 surface.[35,36] Thereafter, multilayer WSe_2 flakes have been exfoliated mechanically from bulk WSe_2 crystals (supplied by 2D Semiconductors, Inc.) and transferred onto the hole arrays in SiO_2/Si substrates with a polydimethylsiloxane (PDMS) stamp[37,38] (see Fig. S2 of the supplementary material).[34] Contact mode AFM (Bruker: MultiMode, Nanoscope IIIa) with a set-point force of ~25 nN has been used to obtain the topography of WSe_2 flakes on substrates and determine the thickness of the flakes. The reason why contact mode instead of tapping mode has been chosen is to provide accurate results for the thickness measurement.[39] The number of layers of the corresponding flakes has been derived by dividing the measured thickness by the interlayer distance. An interlayer distance of 0.70 nm for WSe_2[40,41] has been adopted for calculation.

Fig. 1(a) shows the multilayer WSe_2 flakes, which have been transferred onto the substrate pre-patterned with an array of holes, forming several suspended WSe_2 membranes over the holes. Fig. 1(b) presents the AFM image of the corresponding WSe_2 flake in the square area of Fig. 1(a), while Fig. 1(c) shows the magnified AFM topography image of a suspended area of a 6-layer WSe_2 membrane over a 1.55 μm diameter hole. No visible bubbles, wrinkles, or residue particles have been found on the membranes, which benefits from the appropriate pressure control during the all-dry transfer process.[37] The height profile superimposed in the AFM image of Fig. 1(c) shows a uniform height around the edge of the hole, indicating that the membrane adheres tightly to the edge of the hole possibly by van der Waals interactions (dispersion forces or dipole interactions or both) with the substrate. The Raman measurements have been performed in a confocal Raman spectrometer (inVia Renishaw)

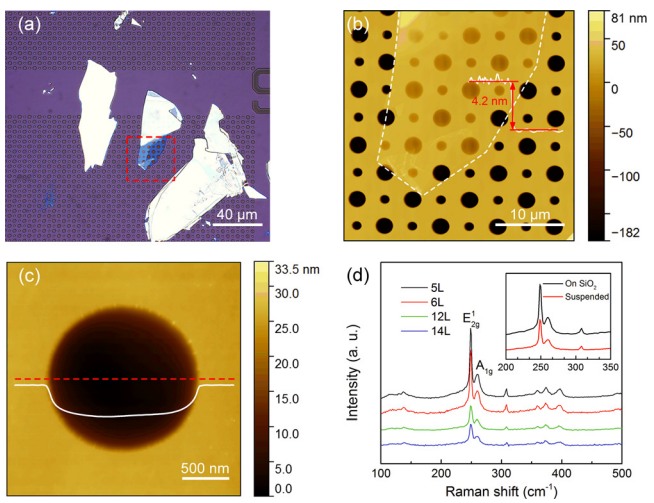

FIG. 1. (a) Optical image of WSe_2 flakes transferred onto pre-patterned SiO_2/Si substrate. (b) AFM image of the corresponding WSe_2 flake inside the square area of (a). (c) AFM image of a WSe_2 membrane suspended over a hole and a superimposed height profile (along the dashed line) shows a step height of ~30 nm. (d) Raman spectra of the suspended WSe_2 flakes with different number of layers in the range of 100–500 cm^{-1}. The inset shows the Raman spectra of supported area and suspended area of a 5-layer WSe_2 flake in the range of 200–350 cm^{-1}. Spectra are offset vertically for clarity.

with a 100× magnification objective in air environment. The wavelength of the laser is 514 nm, and the laser power has been kept at ~0.2 mW. The Raman spectra of the transferred multilayer WSe_2 flakes suspended over the holes are shown in Fig. 1(d). The in-plane mode E^1_{2g} (248.7 cm^{-1}), out-of-plane mode A_{1g} (259.6 cm^{-1}),[42] and a weak peak at 308.2 cm^{-1} arising from the interlayer interaction[40] have been observed. No Raman splitting of the E^1_{2g} mode has been observed, indicating no large strain (>1%) exists in the transferred WSe_2 flakes.[20] The inset of Fig. 1(d) compares the Raman spectra of supported area and suspended area of a 5-layer WSe_2 flake. Peak position shift of E^1_{2g} and A_{1g} modes has not been found, which suggests similar strain exists in the supported and suspended areas.

To obtain the elastic properties of the suspended membranes, indentation experiments have been conducted. Prior to the indentation, the samples have been scanned for 1 h under AFM in order to minimize the thermal drift of the piezoelectric scanner. Then, the tip of an AFM probe with a radius r_{tip} of 81 nm (NuNano: Scout 350 LowRes) has been located in the center of a suspended area of a membrane, and the membrane has been indented with a loading/unloading rate of 100 nm/s repeatedly for several cycles (as illustrated in Fig. 2(a)). During the measurement, no hysteresis has been found in the loading and unloading curves, which indicates that no plastic deformation has occurred to the membranes and the membranes have not slid over the margin of holes. The indentation depth at the center of a membrane has been determined by $\delta = \Delta Z - d$, where ΔZ is the displacement of the piezoelectric scanner as the AFM probe starts to contact with the membrane (see the supplementary material for the determination of contact point),[34] and d is the deflection of the AFM probe. The force applied from the AFM tip onto the membrane has been derived from $F = k \times d$, where k is the spring constant of the corresponding AFM probe (35.7 N/m), which has been calibrated via a reference cantilever with a known spring constant (Bruker: CLFC-NOBO). Representative force F versus displacement ΔZ curves on a suspended WSe_2 membrane and SiO_2/Si substrate are shown in Fig. 2(b). When the AFM probe indents towards the stiff substrate, the probe deflection d is assumed to be equal to the displacement of the scanner ΔZ, which has been used to calibrate the sensitivity of the photodetector of AFM.

Since WSe_2 owns three-fold rotation symmetry and the suspended area of WSe_2 has circular symmetry, each WSe_2 membrane has been modelled as a film with isotropic in-plane mechanical properties. Fig. 2(c) shows the representative force-deformation curves obtained from WSe_2 membranes with different number of layers, which can be approximated with the Schwering-type solution as[2,43,44]

$$F = (\sigma_0^{2D}\pi)\delta + \left(E^{2D}\frac{q^3}{r^2}\right)\delta^3, \quad (1)$$

where σ_0^{2D} is the pretension, r is the radius of the hole, E^{2D} is the 2D elastic modulus, v is the Poisson's ratio (0.19 (Refs. 45 and 46) for WSe_2), and q is a dimensionless constant determined by $q = 1/(1.05 - 0.15v - 0.16v^2)$. With a least square fitting of the experimental data using Eq. (1), the pretension σ_0^{2D} and 2D elastic modulus E^{2D} of the

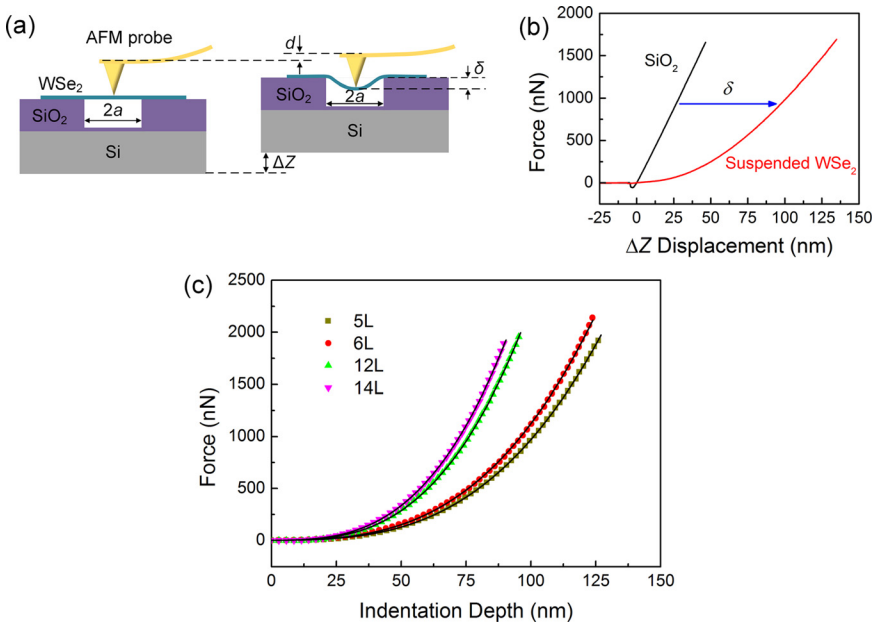

FIG. 2. (a) Schematic of the indentation experiment on a suspended WSe_2 membrane. (b) Force-displacement curves obtained on a suspended WSe_2 membrane and SiO_2/Si substrate. (c) Representative force-deformation curves for suspended WSe_2 membranes with different number of layers. The symbols correspond to the experimental data and the solid lines are fitted curves, agreeing well with the experimental results.

membranes can be derived. The fitted curves (solid lines in Fig. 2(c)) show good agreement with the experimental data, demonstrating the suitability of the chosen mechanic model. From this model, we can see the applied load has an approximate linear relationship with the indentation depth when the membrane deformation is small, while significantly follows a cubic relationship under large deformation.

To determine the variation of the mechanical properties of the suspended WSe_2 membranes, a statistical analysis has been conducted on several WSe_2 flakes with 5, 6, 12, and 14 layers. For each set of layers, the test has been done on 5 membranes with 3 different indentation depths twice, and therefore, 30 force-deformation curves have been obtained, which derives 30 values of σ_0^{2D} and E^{2D} by fitting Eq. (1) to the corresponding force-deformation curves. The results show that both the extracted 2D elastic modulus E^{2D} and pretension σ_0^{2D} are independent of the indentation depth (as shown in Fig. S5 of the supplementary material),[34] which verifies the WSe_2 membranes present an elastic deformation during the indentation experiments. The histograms of the derived 2D elastic modulus E^{2D} and pretension σ_0^{2D} for WSe_2 membranes with different number of layers are shown in Figs. 3(a)–3(d) and Fig. S6 (see the supplementary material),[34] respectively, which can be fitted with the Gaussian distribution. The mean 2D elastic modulus and their standard deviations are 596 ± 23, 690 ± 25, 1411 ± 61, and 1615 ± 56 N/m for 5, 6, 12, and 14-layer thick WSe_2 membranes, respectively, as shown in Fig. 3(e). The deviations are attributed to different defect densities, stacking faults in the membranes, offset of the AFM tip from the center of a membrane, and the curve fitting errors. The 2D elastic modulus of the multilayer WSe_2 membranes has been observed to increase statistically linearly as the number of layers increases. As described previously, the membranes have been found to clamp tightly over the edges of holes (no sliding over the substrates), which indicates interlayer sliding has not happened during the indentation experiments due to the interlayer interaction originating from van der Waals interactions.[47]

In order to compare the elastic properties of 2D WSe_2 with the bulk materials and other materials, the 2D elastic modulus has been converted to the normal 3D Young's modulus E_Y by dividing the 2D value by the thickness of the membranes. Fig. 4(a) shows the box chart of Young's modulus E_Y for WSe_2 membranes with different number of layers. No statistical difference of E_Y among the 4 different WSe_2 membranes has been observed in our results, which indicates the Young's modulus E_Y of the WSe_2 membranes is independent of the thickness. The corresponding values are 170.3 ± 6.7, 166.3 ± 6.1, 167.9 ± 7.2, and 164.8 ± 5.7 GPa for 5, 6, 12, and 14-layer thick WSe_2 membranes, respectively, which is close to the first principle simulation result.[48] Moreover, the mean value of E_Y (167.3 ± 6.7 GPa) for the multilayer WSe_2 membranes is smaller than that of multilayer MoS_2 (~330 GPa),[29] monolayer MoS_2 (~270 GPa),[30,31] monolayer WS_2 (~270 GPa),[31] roughly equal to one sixth of graphene (~1.0 TPa)[1,2] and carbon nanotube (~1.0 TPa),[49] and larger than that of MoS_2 nanotube (~120 GPa).[50] The possible reason for smaller Young's modulus of WSe_2 compared with 2D MoS_2 and WS_2 is that the charge transfer decrease and lattice constant increase in WSe_2 induces the weakening binding between the metal and chalcogen.[46] For a given geometry of NEMS, the resonant frequency will be lower if the Young's modulus of beam is lower or density is higher.[51,52] Thus, 2D WSe_2 with a relatively higher density value (9.32 g/cm^3)[53] and lower Young's modulus compared with other 2D materials can be put into application of NEMS with lower resonance frequency, such as acoustic sensor[54] and loudspeakers.[55] In addition, when flexible electronics composed of 2D materials are bent or stretched, extra stress will be formed at the interface between the 2D material and soft polymeric substrates, due to the mismatch of their mechanical properties, which may weaken the reliability of the devices. 2D WSe_2 with lower Young's modulus will reduce this kind of stress under a certain amount of strain of devices and may therefore be more suitable for flexible electronics applications.

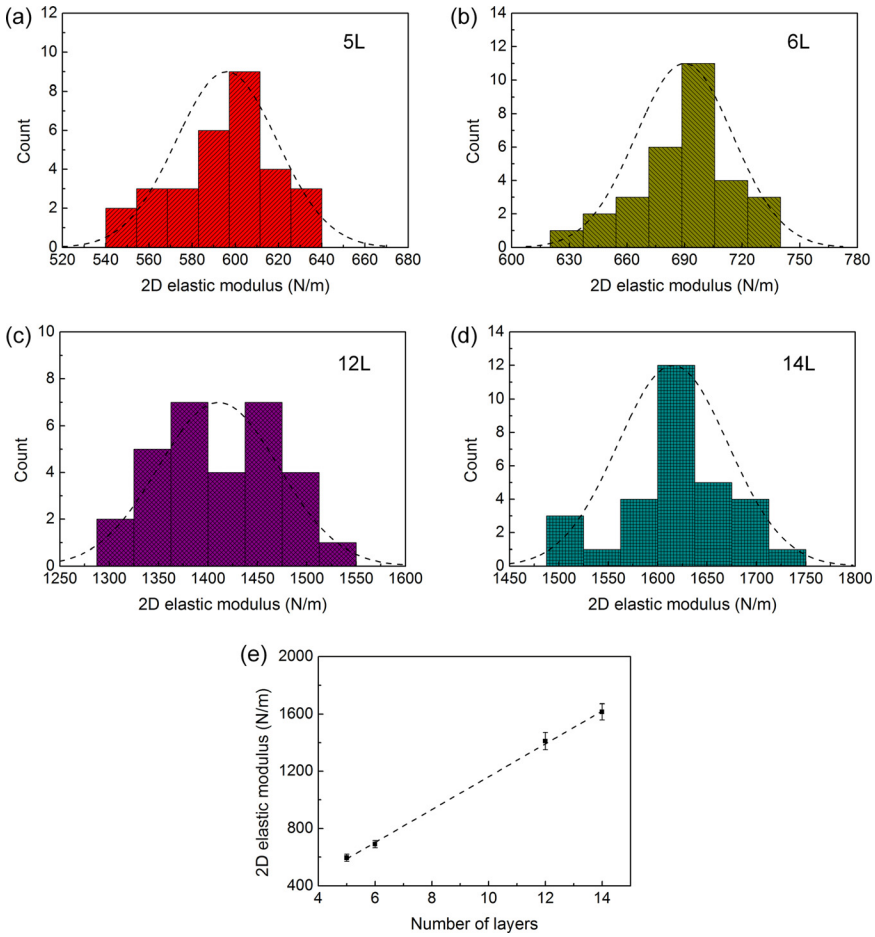

FIG. 3. Histograms of 2D elastic modulus E^{2D} acquired from the curve fitting with Eq. (1) for (a) 5-layer, (b) 6-layer, (c) 12-layer, and (d) 14-layer thick WSe_2 membranes. The dashed lines indicate the fitted Gaussian distributions. (e) 2D elastic modulus E^{2D} of WSe_2 membranes as a function of the number of layers. The error bars represent the standard deviations.

During the whole indentation experiments, the maximum force applied on these WSe_2 membranes is ~3200 nN. None of the membranes have been fractured and all still kept their original elastic properties under this force. The maximum stress for a circular and linear elastic membrane during an indentation experiment with a spherical indenter in the case of $r_{tip}/r \ll 1$ can be derived with the expression as[56]

$$\sigma_{max}^{2D} = \sqrt{\frac{F_{max}E^{2D}}{4\pi r_{tip}}}. \quad (2)$$

Thus, the maximum stress for a 5-layer WSe_2 membrane is calculated to be ~43 N/m, corresponding to ~12.4 GPa. Assuming the stress of multilayer WSe_2 has a linear relationship with its strain ($\sigma = E_Y\varepsilon$) results in the maximum strain of approximate 7.3%. Thus, the multilayer WSe_2 can at least withstand ~12.4 GPa stress and ~7.3% strain without breaking. (The breaking stress/strain is larger than ~12.4 GPa/~7.3%.) This means the breaking strain of 2D WSe_2 is at least three times larger than that of silicon (0.4%–2.2%)[57] and comparable with the common materials used for substrates of flexible electronics, namely, polyimide (PI) or PDMS (~7%),[58] implying that 2D WSe_2 is compatible with most of flexible electronic devices.

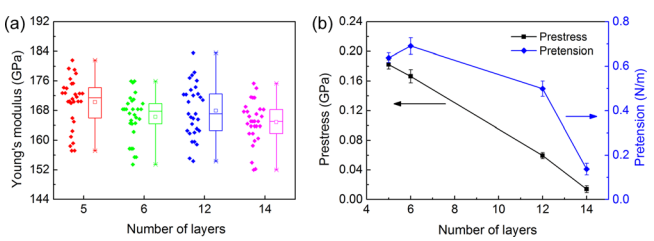

FIG. 4. (a) The box chart of Young's modulus E_Y for WSe_2 membranes with different number of layers. Each plot includes the minimum, lower quartile, median (horizontal line), mean (hollow square), upper quartile, maximum, and discrete data at the left. (b) Pretension and prestress for the corresponding multilayer WSe_2 membranes.

Fig. 4(b) shows the relationship between the extracted pretension and prestress (pretension divided by the thickness of the membranes) and the number of layers of WSe_2 membranes. As can be seen, in our experiments, the pretension σ_0^{2D} varies with the thickness of WSe_2 membranes and is in the same scale as the reports of Refs. 29 and 31, which employ a similar 2D materials transfer method. In addition, the prestress that originates from the mechanical exfoliation and transfer process decreases approximately linearly as the number of layers increases. During the transfer process, the pressing of PDMS stamp together with WSe_2 would have resulted in the PDMS stamp expanding laterally (see Fig. S2(c) of the supplementary material),[34] due to the softness of the PDMS,[59] which could have stretched the WSe_2 flakes to a certain extent. When the PDMS stamp has been peeled off from the substrate, it is likely that the stretched WSe_2 flakes adhering to the substrate by van der Waals force result in the positive pretension formed in the transferred flakes.

In conclusion, we have fabricated multilayer WSe_2 membranes suspended over circular holes. The elastic properties of WSe_2 membranes with different number of layers

have been determined employing nanoindentation experiments. The results show that although the prestress decreases approximately linearly as the number of layers increases, the Young's modulus is independent of the number of layers, which indicates the interlayer interaction is strong enough to prevent the interlayer sliding. The Young's modulus of multilayer WSe_2 is about two thirds of other most investigated 2D semiconducting TMDs, namely, MoS_2 and WS_2, and one sixth of graphene and carbon nanotube. During the experiments, the WSe_2 membranes have withstood ~12.4 GPa stress and ~7.3% strain without breaking or mechanical degradation. 2D WSe_2 can be an attractive alternative for graphene in some applications requiring flexible semiconducting materials, such as bendable transistors, photodetectors, photovoltaics, and NEMS.

We would like to thank the financial support of UK Engineering and Physical Sciences Research Council (EPSRC) for this work. We acknowledge Atif Syed's assistance with the AFM tip characterization.

[1]G.-H. Lee, R. C. Cooper, S. J. An, S. Lee, A. van der Zande, N. Petrone, A. G. Hammerberg, C. Lee, B. Crawford, W. Oliver, J. W. Kysar, and J. Hone, Science **340**, 1073 (2013).
[2]C. Lee, X. Wei, J. W. Kysar, and J. Hone, Science **321**, 385 (2008).
[3]K. S. Novoselov, A. K. Geim, S. Morozov, D. Jiang, Y. Zhang, S. a. Dubonos, I. Grigorieva, and A. Firsov, Science **306**, 666 (2004).
[4]S. Bae, H. Kim, Y. Lee, X. Xu, J.-S. Park, Y. Zheng, J. Balakrishnan, T. Lei, H. R. Kim, Y. I. Song, Y.-J. Kim, K. S. Kim, B. Ozyilmaz, J.-H. Ahn, B. H. Hong, and S. Iijima, Nat. Nanotechnol. **5**, 574 (2010).
[5]K. S. Kim, Y. Zhao, H. Jang, S. Y. Lee, J. M. Kim, K. S. Kim, J.-H. Ahn, P. Kim, J.-Y. Choi, and B. H. Hong, Nature **457**, 706 (2009).
[6]A. M. van der Zande, R. A. Barton, J. S. Alden, C. S. Ruiz-Vargas, W. S. Whitney, P. H. Q. Pham, J. Park, J. M. Parpia, H. G. Craighead, and P. L. McEuen, Nano Lett. **10**, 4869 (2010).
[7]C. Y. Chen, S. Rosenblatt, K. I. Bolotin, W. Kalb, P. Kim, I. Kymissis, H. L. Stormer, T. F. Heinz, and J. Hone, Nat. Nanotechnol. **4**, 861 (2009).
[8]J. S. Bunch, A. M. van der Zande, S. S. Verbridge, I. W. Frank, D. M. Tanenbaum, J. M. Parpia, H. G. Craighead, and P. L. McEuen, Science **315**, 490 (2007).
[9]Y. Zhang, Y.-W. Tan, H. L. Stormer, and P. Kim, Nature **438**, 201 (2005).
[10]W. Zhao, Z. Ghorannevis, L. Chu, M. Toh, C. Kloc, P.-H. Tan, and G. Eda, ACS Nano **7**, 791 (2013).
[11]Q. H. Wang, K. Kalantar-Zadeh, A. Kis, J. N. Coleman, and M. S. Strano, Nat. Nanotechnol. **7**, 699 (2012).
[12]J. Yoon, W. Park, G.-Y. Bae, Y. Kim, H. S. Jang, Y. Hyun, S. K. Lim, Y. H. Kahng, W.-K. Hong, B. H. Lee, and H. C. Ko, Small **9**, 3295 (2013).
[13]H. Wang, L. L. Yu, Y. H. Lee, Y. M. Shi, A. Hsu, M. L. Chin, L. J. Li, M. Dubey, J. Kong, and T. Palacios, Nano Lett. **12**, 4674 (2012).
[14]S. Bertolazzi, D. Krasnozhon, and A. Kis, ACS Nano **7**, 3246 (2013).
[15]O. Lopez-Sanchez, D. Lembke, M. Kayci, A. Radenovic, and A. Kis, Nat. Nanotechnol. **8**, 497 (2013).
[16]J. S. Ross, P. Klement, A. M. Jones, N. J. Ghimire, J. Yan, D. G. Mandrus, T. Taniguchi, K. Watanabe, K. Kitamura, W. Yao, D. H. Cobden, and X. Xu, Nat. Nanotechnol. **9**, 268 (2014).
[17]A. Pospischil, M. M. Furchi, and T. Mueller, Nat. Nanotechnol. **9**, 257 (2014).
[18]S. Wi, M. Chen, D. Li, H. Nam, E. Meyhofer, and X. Liang, Appl. Phys. Lett. **107**, 062102 (2015).
[19]S. Wi, H. Kim, M. K. Chen, H. Nam, L. J. Guo, E. Meyhofer, and X. G. Liang, ACS Nano **8**, 5270 (2014).
[20]S. B. Desai, G. Seol, J. S. Kang, H. Fang, C. Battaglia, R. Kapadia, J. W. Ager, J. Guo, and A. Javey, Nano Lett. **14**, 4592 (2014).
[21]H. J. Conley, B. Wang, J. I. Ziegler, R. F. Haglund, S. T. Pantelides, and K. I. Bolotin, Nano Lett. **13**, 3626 (2013).
[22]A. D. Smith, F. Niklaus, A. Paussa, S. Vaziri, A. C. Fischer, M. Sterner, F. Forsberg, A. Delin, D. Esseni, P. Palestri, M. Östling, and M. C. Lemme, Nano Lett. **13**, 3237 (2013).
[23]D. Ovchinnikov, A. Allain, Y. S. Huang, D. Dumcenco, and A. Kis, ACS Nano **8**, 8174 (2014).
[24]N. Perea-López, A. L. Elías, A. Berkdemir, A. Castro-Beltran, H. R. Gutiérrez, S. Feng, R. Lv, T. Hayashi, F. López-Urías, S. Ghosh, B. Muchharla, S. Talapatra, H. Terrones, and M. Terrones, Adv. Funct. Mater. **23**, 5511 (2013).
[25]S. Das and J. Appenzeller, Appl. Phys. Lett. **103**, 103501 (2013).
[26]T. Yan, X. Qiao, X. Liu, P. Tan, and X. Zhang, Appl. Phys. Lett. **105**, 101901 (2014).
[27]H. Fang, S. Chuang, T. C. Chang, K. Takei, T. Takahashi, and A. Javey, Nano Lett. **12**, 3788 (2012).
[28]B. Radisavljevic, A. Radenovic, J. Brivio, V. Giacometti, and A. Kis, Nat. Nanotechnol. **6**, 147 (2011).
[29]A. Castellanos-Gomez, M. Poot, G. A. Steele, H. S. J. van der Zant, N. Agrait, and G. Rubio-Bollinger, Adv. Mater. **24**, 772 (2012).
[30]S. Bertolazzi, J. Brivio, and A. Kis, ACS Nano **5**, 9703 (2011).
[31]K. Liu, Q. M. Yan, M. Chen, W. Fan, Y. H. Sun, J. Suh, D. Y. Fu, S. Lee, J. Zhou, S. Tongay, J. Ji, J. B. Neaton, and J. Q. Wu, Nano Lett. **14**, 5097 (2014).
[32]M. M. Benameur, B. Radisavljevic, J. S. Heron, S. Sahoo, H. Berger, and A. Kis, Nanotechnology. **22**, 125706 (2011).
[33]P. Blake, E. W. Hill, A. H. Castro Neto, K. S. Novoselov, D. Jiang, R. Yang, T. J. Booth, and A. K. Geim, Appl. Phys. Lett. **91**, 063124 (2007).
[34]See supplementary material at http://dx.doi.org/10.1063/1.4940982 for the details of patterning of SiO_2/Si substrate, exfoliation, and transfer process of multilayer WSe_2, characterization of AFM tip, calibration of force-deformation curves, 2D elastic modulus and pretension at different indentation depths, and pretension distribution for WSe_2 membranes.
[35]Y. Huang, E. Sutter, N. N. Shi, J. Zheng, T. Yang, D. Englund, H.-J. Gao, and P. Sutter, ACS Nano **9**, 10612 (2015).
[36]K. Nagashio, T. Yamashita, T. Nishimura, K. Kita, and A. Toriumi, J. Appl. Phys. **110**, 024513 (2011).
[37]A. Castellanos-Gomez, M. Buscema, R. Molenaar, V. Singh, L. Janssen, H. S. J. van der Zant, and G. A. Steele, 2D Mater. **1**, 011002 (2014).
[38]M. A. Meitl, Z. T. Zhu, V. Kumar, K. J. Lee, X. Feng, Y. Y. Huang, I. Adesida, R. G. Nuzzo, and J. A. Rogers, Nat. Mater. **5**, 33 (2006).
[39]P. Nemes-Incze, Z. Osváth, K. Kamarás, and L. P. Biró, Carbon **46**, 1435 (2008).
[40]H. Li, G. Lu, Y. Wang, Z. Yin, C. Cong, Q. He, L. Wang, F. Ding, T. Yu, and H. Zhang, Small **9**, 1974 (2013).
[41]W. Liu, J. Kang, D. Sarkar, Y. Khatami, D. Jena, and K. Banerjee, Nano Lett. **13**, 1983 (2013).
[42]D. G. Mead and J. C. Irwin, Can. J. Phys. **55**, 379 (1977).
[43]U. Komaragiri, M. R. Begley, and J. G. Simmonds, J. Appl. Mech. **72**, 203 (2005).
[44]M. R. Begley and T. J. Mackin, J. Mech. Phys. Solids. **52**, 2005 (2004).
[45]J. Kang, S. Tongay, J. Zhou, J. Li, and J. Wu, Appl. Phys. Lett. **102**, 012111 (2013).
[46]F. Zeng, W.-B. Zhang, and B.-Y. Tang, Chin. Phys. B **24**, 097103 (2015).
[47]M. Kertesz and R. Hoffmann, J. Am. Chem. Soc. **106**, 3453 (1984).
[48]L.-P. Feng, N. Li, M.-H. Yang, and Z.-T. Liu, Mater. Res. Bull. **50**, 503 (2014).
[49]M. F. Yu, B. S. Files, S. Arepalli, and R. S. Ruoff, Phys. Rev. Lett. **84**, 5552 (2000).
[50]A. Kis, D. Mihailovic, M. Remskar, A. Mrzel, A. Jesih, I. Piwonski, A. J. Kulik, W. Benoît, and L. Forró, Adv. Mater. **15**, 733 (2003).
[51]L. Sekaric, J. M. Parpia, H. G. Craighead, T. Feygelson, B. H. Houston, and J. E. Butler, Appl. Phys. Lett. **81**, 4455 (2002).
[52]Y. T. Yang, K. L. Ekinci, X. M. H. Huang, L. M. Schiavone, M. L. Roukes, C. A. Zorman, and M. Mehregany, Appl. Phys. Lett. **78**, 162 (2001).
[53]M. K. Agarwal and P. A. Wani, Mater. Res. Bull. **14**, 825 (1979).
[54]E. Grady, E. Mastropaolo, T. Chen, A. Bunting, and R. Cheung, Microelectron. Eng. **119**, 105 (2014).
[55]J. W. Suk, K. Kirk, Y. Hao, N. A. Hall, and R. S. Ruoff, Adv. Mater. **24**, 6342 (2012).
[56]N. M. Bhatia and W. Nachbar, Int. J. Nonlinear Mech. **3**, 307 (1968).
[57]T. Ando, K. Sato, M. Shikida, T. Yoshioka, Y. Yoshikawa, and T. Kawabata, paper presented at Proceedings of the 1997 International Symposium on Micromechatronics and Human Science (1997).
[58]D.-H. Kim, J.-H. Ahn, W. M. Choi, H.-S. Kim, T.-H. Kim, J. Song, Y. Y. Huang, Z. Liu, C. Lu, and J. A. Rogers, Science **320**, 507 (2008).
[59]I. D. Johnston, D. K. McCluskey, C. K. L. Tan, and M. C. Tracey, J. Micromech. Microeng. **24**, 035017 (2014).